(NASA-CR-164340) QUANTITATIVE ABSORPTION AND FLUORESCENCE STUDIES OF NO BETWEEN 1060 AND 2000 A (SRI International Corp., Menlo Park, Calif.) 29 p HC A03/MF A01 CSCL 20H

N81-23867

Unclas
G3/72 15007

QUANTITATIVE ABSORPTION AND FLUORESCENCE STUDIES OF NO BETWEEN 1060 AND 2000 Å

J A Guest and L C Lee
Molecular Physics Laboratory
SRI International
Menlo Park, California 94025
U. S. A.

ABSTRACT

Synchrotron radiation in the 1060-2000 Å region has been used to measure the average absorption and fluorescence cross sections of NO and to determine approximate photodissociation quantum yields. Several vibrational levels of the $D^2\Sigma^+$, $E^2\Sigma^+$, and $B'^2\Delta$ states have high fluorescence quantum yields. The $C^2\Pi$ and $B^2\Pi$ states do not fluoresce when the excitation energies are above the first dissociation limit, in accord with previous experiments. In general, the fluorescence yields decrease with increasing photon energy. The present quantitative measurements are compared with spectroscopic observations and are found to be reasonably consistent.

MP 80-153
02/11/81

1. INTRODUCTION

Nitric oxide has been the subject of much scientific inquiry, both to seek a fundamental understanding of its spectroscopy and to ascertain its role in the chemistry of the upper atmosphere and of air pollution. Recently, NO has been found in instellar space (Liszt and Turner 1978), so its photodissociation cross section in the vacuum ultraviolet region is useful for determining its destruction rate.

Miescher and coworkers (Miescher and Huber 1976, and references therein) have been largely responsible for unraveling the complex high resolution vacuum-UV spectroscopy of NO over the past 25 years. Absorption bands down to 1250 Å have been well assigned (Miescher and Alberti 1976). Quantitative absorption measurements of NO in the vacuum UV have been performed by Marmo (1953) and by Watanabe, Matsunaga, and Sakai (1967), who have measured accurate absorption and photoionization cross sections for NO at wavelengths shorter than 1350 Å.

Many absorption bands of NO have sharp rotational structure at energies above the first dissociation limit. These narrow line widths make cross section measurements difficult because of the intensity and bandwidth limitations of the continuum VUV light sources currently available. At light source bandwidths greater than rotational line widths, the lower limits of the absorption cross section averaged over the bandwidth can be determined at low pressures where the rotational transitions are not saturated. We have measured average absorption cross sections for NO from 2000 Å to 1350 Å and the true absorption cross sections from 1350 Å to 1060 Å.

At excitation energies above the first dissociation limit, several NO bands still fluoresce. Young, Black, and Slanger (1968) dispersed the visible

emission from several electronic states of NO at 1470 Å excitation. They observed no visible fluorescence at energies above the first ionization limit. We have also studied total NO molecular fluorescence in the UV and present here quantitative excitation spectra. The photodissociation cross section has been determined from the difference of the total absorption cross section and the fluorescence cross section.

2. EXPERIMENTAL

Synchrotron radiation produced at the University of Wisconsin electron storage ring provided continuum light in the vacuum ultraviolet (VUV) region. The incident light was dispersed through a one-meter vacuum monochromator (McPherson 225) with a 600 ℓ/mm aluminum grating, permitting a highest resolution of 0.3 Å. A 2-mm LiF window separated the monochromator from the experimental cell. The experimental cell was a low-flow system pumped continuously with a sorption pump. Pressures from 0.2 to 65 mtorr were measured using an MKS capacitance manometer. The NO used was obtained from Liquid Carbonic with a minimum purity of 99% and was used without further purification. We remeasured some cross sections using static gas conditions, and the results agreed with the flowing gas cross sections. We prefer the flow system to keep a fresh supply of NO in the cell at all times and to remove photodissociation products. The measurements were performed at a room temperature of 20° C.

Absorption was measured by the light attenuation as a function of pressure at each wavelength. The attenuated and the incident light intensities were converted to logs, chopped, and compared using a lock-in amplifier (PAR HR-8) as described previously (Lee 1980). The absorption cross

section, σ, was computed directly from the slope of $\ln(I_o/I)$ versus pressure at each wavelength, where I_o and I are the incident and attenuated photon fluxes, respectively. Figure 1 plots $\ln(I_o/I)$ as a function of pressure, P, at several different wavelengths. When the incident light bandwidth is larger than the molecular absorption width, the absorption relation will deviate from Beer's law. At 1406 Å, the NO rotational lines are probably broadened by predissociation, and Beer's law is followed to high pressures. At 1499 and 1605 Å, the rotational lines are much narrower than the minimum monochromator bandwidth of 0.3 Å. These absorptions still obey Beer's Law to higher pressures, perhaps because they have smaller oscillator strengths and require higher pressures to saturate. At 1731 and 1829 Å, the rotational lines are narrow and have high cross sections, so the absorption deviates from Beer's law at pressures higher than 2 mtorr.

Since the exciting light bandwidth will cover several rotational lines of different absorption cross sections, the measured cross sections will depend on the monochromator bandwidth. The absorptions at 1829 and 1832.5 Å were measured at various monochromator bandwidths from 0.3 to 1.8 Å. The value of $\ln(I/I_o)$ increases, as expected, with better resolution, but since the manifold of rotational states is so dense and the rotational lines are so narrow, the effect of resolution on $\ln(I_o/I)$ is not dramatic.

NO molecular fluorescence was detected at right angles to the excitation source and 7 cm from the exit slit of the monochromator. UV fluorescence was measured using a partially solar-blind EMI G26H215 photomultiplier (PMT) tube with a CsTe cathode and MgF_2 window with an ORTEC counting system. Figure 2 plots the PMT quantum efficiency as a function of wavelength. The PMT was coupled directly to the cell to permit observation of fluorescence to the MgF_2 cutoff (~ 1150 Å). An EMI 9558QB PMT with a glass filter was used to detect

near UV and visible fluorescence ($\lambda > 3000$ Å) using the same cell geometry. All fluorescence measurements were made using a 1 Å excitation bandpass.

The synchrotron radiation photon flux entering the gas cell for each mA of electron beam current and 1 Å monochromator bandwidth is also shown in Figure 2. The electron beam current starts at 100 mA and decreases with time to 40 mA in about three hours. The light intensity was measured using a freshly prepared sodium salicylate/photomultiplier combination and a calibrated EMR photodiode.

3. RESULTS

3.1 Absorption cross section

When excited molecular states predissociate or ionize, the band's rotational lines become sufficiently diffuse in absorption to permit measurement of accurate absorption cross sections at the currently available resolution. At energies near and above the first ionization limit of 9.266 eV, we measure true absorption cross sections because the absorption bands are very diffuse. At longer wavelengths, the absorption measured can be evaluated only as average cross sections for a given instrumental bandwidth.

Absorption cross sections at 0.3 Å resolution are presented in figures 3 thourgh 6. The wavelengths of the states assigned by various investigators (Dressler and Miescher 1965, Jungen 1966, Lagerquist and Miescher 1966, Lofthus and Miescher 1964, Miescher 1966 and 1971, Miescher and Huber 1976, Ng, Mahan and Lee 1976, Tanaka 1953) are indicated in the figures for identification. Between 1100 and 1350 Å (Fig. 3), the absolute absorption cross sections measured here are in good agreement with those measured by Watanabe et al (1967) to within 30%. The present cross sections between 1100-

1050 Å compared less well to those of Watanabe. At wavelengths shorter than 1400 Å, the present cross sections also agree reasonably well with those of Marmo (1953). But at wavelengths longer than 1400 Å, the present absorption cross sections became systematically larger, up to a 50-fold increase. This apparent disagreement stems from pressure and light bandwidth effects discussed previously. At the high pressures Marmo used, the absorption lines were completely saturated. In addition, his spectral bandwidth was 1 Å, significantly broader than that in the present work.

Although our measured absorption cross sections are large, they are still considered to be average cross sections because of our limited resolution. Integrated cross sections for some of the longer wavelength NO absorption bands have been measured by both pressure-broadening (Bethke 1959) and dispersion techniques (Farmer, Hasson and Nicholls 1972). The cross sections determined by those two methods are self-consistent. We compare the present results by assuming that our absorption bands are triangles with half-width $\Delta\nu$, and

$$K_o = \bar{\sigma}_{max} \Delta\nu / 3.7 \times 10^{-2}$$

where $\bar{\sigma}_{max}$ is the peak cross section in Mb, 3.7×10^{-2} converts the cross section to units of cm^{-1} atm^{-1}, and K_o is the approximate integrated cross section in units of cm^{-2} atm^{-1}.

Our results for the integrated absorption cross sections are from 10% to 30% higher than Bethke's integrated cross sections (see Table 1) for the β, γ, and ε systems, but are about a factor of 2 higher for the δ system. Callear and Pilling (1970) indicated that Bethke's results for the ε system were confirmed, but results for the δ system were too small by a factor of ~ 2.3. This comparisor strengthens the validity of our absorption measurements using the linear region of $\ln(I_o/I)$ versus pressure despite band-

width limitations. Farmer, et al (1968) have similarly determined oscillator strengths for the Schumann-Runge system of O_2 using incident light with limited resolution.

Cross sections of individual rotational lines can be measured only when the monochromator bandwidth is smaller than the rotational line width. Since this is not possible in the present case, a way to estimate the true rotational line cross sections from the present measurements would be useful. Cieslik and Nicolet (1973) have used relative rotational line intensities and known integrated cross sections for some bands to compute cross sections for rotational lines of some NO bands from the relation

$$\int_{J'-J''} \sigma(\nu)d\nu = \frac{\pi e^2}{mc^2} f(J'J'') \frac{n_{J''}}{n}$$

where f(J', J") is the oscillator strength for the $J' \leftarrow J''$ transition ($J' = J''$, $J'' \pm 1$), $n_{J''}$ is the population of the molecules in the J" rotational level, and n is the gas concentration. For the $C^2\Pi$ (v = 0) absorption, the peak rotational cross section is found to be about 2.3×10^{-16} cm^2 by Cieslik and Nicolet (1973) and 10^{-16} cm^2 by Frederick and Hudson (1979). These results indicate that the true cross sections for individual (sharp) rotational lines are several times larger than those measured in the current study.

The average absorption cross sections of this study could be converted to individual rotational line cross sections as follows. The light transmitted at wavelength λ_o is given by

$$I = \int I_o g(\lambda) e^{-n\sigma(\lambda)\ell} d\lambda$$

where I_o is the incident photon intensity, $g(\lambda)$ is the monochromator bandwidth function with $\int g(\lambda)d\lambda = 1$, and the integration is over the monochromator bandwidth, $\Delta\lambda$.

At low gas pressure, where $e^{-n\sigma(\lambda)\ell} \sim 1 - n\sigma(\lambda)\ell$, we have

$$I \simeq I_o[1 - n\ell\int g(\lambda)\sigma(\lambda)d\lambda]$$

or

$$\ell n(I_o/I) \simeq n\ell\int g(\lambda)\sigma(\lambda)d\lambda$$

If we know the number and identity of rotational lines within our bandwidth, we can calculate the relative σ values for each line from the Honl-London factors (Cieslik and Nicolet 1973) for the transition. The relative absorption cross sections can be put into absolute scale by normalization to the measured average absorption cross section

$$\bar{\sigma} = \int g(\lambda)\sigma(\lambda)d\lambda$$

for the band.

3.2 Fluorescence cross sections

The fluorescence cross section, σ_f, can be determined from the radiation rate at low gas pressure, which is

$$\dot{n}_f = K\sigma_f n I_o$$

where K is a geometrical factor determined by comparison with a similar system having a known fluorescence cross section.

Cross sections for the production of UV fluorescence from NO are presented in Figures 4, 5, and 6. No fluorescence was detected in the 1060-1350 Å excitation region (fig. 3). The fluorescence cross sections were measured at 1 Å bandwidth and are normalized to the absorption cross section of the $D^2\Sigma^+(0) \leftarrow X^2\Pi(0)$ transition. The $D^2\Sigma^+$ state is known to not dissociate. The only process that competes with the direct D-X emission is the D-A infrared emission at ~ 11000 Å with a radiative rate three to four times slower than that of the $D \rightarrow X$ emission (Callear and Pilling 1970, Lahmani et al 1981). The Franck-Condon factors for the $D \rightarrow A$ transition are nearly diagonal (Nicholls, 1964), so $A^2\Sigma^+(0)$ is produced by radiation from $D^2\Sigma^+(0)$. Experimental (Engleman et al. 1970) and theoretical (Nicholls, 1964) Franck-Condon factors can be used to estimate the fraction of fluorescence in the response region of the solar blind photomultiplier whose quantum efficiency is known. It is estimated that the photomultiplier observes about 70% for the $A^2\Sigma^+(3) \rightarrow X^2\Pi(v'')$ emission, and more than 95% for the $D^2\Sigma^+(0) \rightarrow X^2\Pi(v'')$ emission. The observed quantum yield for the NO uv fluorescence at 1873 Å excitation can thus be only a few percent less than unity.

The geometrical constant K obtained for the UV fluorescence of NO agrees with that obtained from the $A^1\Pi(1) \rightarrow X^1\Sigma^+(0)$ fluorescence of CO in the same experiment (Lee and Guest 1981). Since the $A^1\Pi(1)$ state of CO is below the dissociation limit, its fluorescence quantum yield equals 1. The agreement of these results lends confidence to the use of the unity fluorescence yield for the $D^2\Sigma^+(0)$ to normalize the NO fluorescence data.

Error limits to the fluorescence cross sections measured can be estimated

from uncertainties in pressure and incident photon flux and from systematic errors caused by variations of the PMT quantum efficiency with wavelength. This last effect depends on the spectral region of the UV fluorescence and varies systematically for each excitation band. For example, the $A^2\Sigma^+(3)$ state has energy below the dissociation limit, so its fluorescence yield must be unity. But, as shown in Fig. 6, the $A^2\Sigma^+(3) \rightarrow X^2\Pi(0)$ transition shows a fluorescence quantum yield smaller than unity. This is because some of the $A^2\Sigma^+(3) \rightarrow X^2\Pi(v")$ fluorescence is in the wavelength region where the quentum efficiency of the solar blind photomultiplier drops. As mentioned above, only about 70% of the $A^2\Sigma^+(3) \rightarrow X^2\Pi(v")$ fluorescence is observed by the photomultiplier which agrees with experimental observation. Such detector errors may cause up to ± 30% uncertainty in the relative values of the fluorescence cross sections.

Since the UV fluorescence cross sections are normalized to our average absorption cross sections, they are not true absolute cross sections. Since all the bands that do emit have sharp rotational structure, the true fluorescence cross sections per rotational line should be several times larger, by analogy to the absorption cross section case. The fluorescence in the near UV and visible region ($\lambda > 3000$ Å) is generally negligible, since the cross sections for visible emission are never greater than 0.5 Mb.

Our visible fluorescence results deserve some mention. Cross sections for visible emission were determined by comparison with $OH(A^2\Sigma^+ \rightarrow X^2\Pi)$ emission from photodissociation of H_2O (Lee, 1980). At low pressures (< 10 mtorr), where secondary reactions are less likely, the upper limit to visible emission is about 0.5 Mb and in most cases is far smaller. The visible fluorescence band shapes are similar to those in the UV and are not presented graphically here. In all cases, the same states that emit in the UV

also emit in the visible, but are lower in intensity by at least a factor of 50-60. Much of this emission is very likely due to fluorescence to higher vibrational levels of the $X^2\Pi$ state at $\lambda > 3000$ Å. The only significant variation from the UV emission pattern occurs at the $E^2\Sigma^+ 4s\sigma$ absorptions. At these positions, the UV emission is only about 12 times more intense than the visible emission. The Rydberg-Rydberg $E4s\sigma \rightarrow A3s\sigma$ transition centered at 6000 Å (Miescher, 1971) probably produces the visible emission.

3.3 Fluorescence quantum yield

The fluorescence quantum yield is the ratio of fluorescence cross section to absorption cross section, $\eta = \sigma_f/\sigma$. If all the rotational lines in a vibrational band can be assumed to have the same fluorescence yield, then the measured yield will be equal to the true quantum yield for the rotational lines. The UV fluorescence quantum yields for all the absorption peaks are shown in Figure 7. The photoionization yields given by Watanabe et al (1967) are also shown in Figure 7.

The excited states that do not fluoresce presumably dissociate. This has been recently confirmed by Slanger (1980), who observed that O atoms are produced from the $NO(C^2\Pi_1\ v > 0)$ state. Therefore, the photodissociation yield can be estimated from the (1 - fluorescence yield), the scale for which is also indicated in Figure 7. The accuracy of the photodissociation yield is limited by the uncertainty of the fluorescence yield.

4. DISCUSSION

The presence or absence of UV fluorescence from NO is basically consistent with spectroscopic observation. The following discussion of the UV fluorescence is divided into sections dealing with states of $^2\Sigma$, $^2\Pi$, and $^2\Delta$ symmetries that fluoresce.

4.1 $^2\Sigma$ States

Since the lower vibrational levels of the $NO(A^2\Sigma^+, 3s\sigma)$ Rydberg state are spectroscopically accessible by photon wavelengths longer than air cutoff, they have been much studied. The $3s\sigma(3)$ band, which lies below the first dissociation limit, fluoresces in the UV. Emissions from the $A^2\Sigma^+$ $v > 3$ levels are rarely reported. They may not be significantly produced because of small Franck-Condon factors for the $A^2\Sigma^+(v > 3) \leftarrow X^2\Pi\ (v = 0)$ transitions (Spindler, Isaacson, and Wentink 1970), or they may be predissociated.

The $D^2\Sigma^+(3p\sigma)$ Rydberg state of NO has been used here to normalize the UV fluorescence cross sections. The $3p\sigma$ ($v' = 0, 1, 2, 3$ levels) all show high fluorescence in the UV, although the apparent yields progressively drop with increasing vibrational number. It is likely that this decrease is caused by partial predissociation. Brzozowski, Erman, and Lyyra (1976) have measured the lifetimes for the $3p\sigma$ ($v = 0$, 1, 2 and 3) vibrational levels to be 24.6, 25.8, 19.8, and 14.2 ns, and their predissociation rates to be ~ 0, $< 2 \times 10^6$, 1.8×10^7, and 4.0×10^7 sec^{-1}, respectively. It is also possible that the decrease of fluorescence yields may be caused partly by the systematic error in the detection system or by the presence of dissociative states at the same energy. At $v = 4$, the apparent fluorescence yield drops below 30%, but the overlap with the $3d\delta(0)$ level makes analysis difficult. Above $v = 4$,

the 3pσ state does not fluoresce in the UV. These bands may be completely predissociated, although this is not indicated in the literature.

The $E^2\Sigma^+$ (4sσ) state also fluoresces strongly in the UV at v = 0 and v = 1, with about a 50% quantum yield. At v = 2, the yield appears to drop to below 30%, but overlapping with the B'Δ(5) level makes a quantitative analysis difficult. At v = 3 and 4, the 4sσ rotational structure is known to be broad, and NO presumably dissociates upon absorption into these states. The E-A emission band is also absent above v = 2. The v = 5 level is missing in absorption as well as emission. The $M^2\Sigma^+$(4pσ) v = 0 state may fluoresce, but its overlap with the $B'^2\Delta(4)$ and 3dδ(1) states makes analysis difficult.

4.2 $^2\Pi$ States

Most $^2\Pi$ states of NO are known to predissociate strongly above the first dissociation limit. Among these are the well-studied $B^2\Pi$ valence and $C^2\Pi$ (3pπ) Rydberg states. Some rotational levels of the 3pπ (v = 0) Rydberg state lie below the first dissociation limit and give weak emission at about 1909 Å, as shown in Figure 4. The UV fluorescence yield for this level is not greater than 10%. Emission to the wavelength where the PMT is insensitive is unlikely, considering the energy distribution in the low-pressure fluorescence emission spectrum of Lahmani et al (1981). We also find that the 3pπ(1) band does not fluoresce at low pressures, in agreement with Lahmani et al (1981). Other studies have indicated that the 3pπ(1) state has a weak fluorescence upon photon excitation (Benoist D'Azy et al 1975, Asher and Haas 1978), but the NO pressures used may have been too high to permit fluorescence under collision-free conditions.

The $H'^2\Pi(3d\pi)$ Rydberg state is known to emit in the visible to the $A^2\Sigma$ state under discharge excitation conditions (Miescher 1971, Huber 1964). The $3d\pi$ v = 0 and v = 1 states are weak in absorption, but they appear to emit in the UV with quantum efficiencies of more than 20%. The H' → X transition may thus be expected to be observable from discharge emission.

4.3 $^2\Delta$ States

The states with $^2\Delta$ symmetry are noted to be most stable with respect to predissociation from discharge emission studies, and several of these levels appear in our fluorescence spectra. The $B'^2\Delta$ valence state, with its long vibrational progression, is the most prominent in emission here. The $B'^2\Delta(0)$ state overlaps the strong $3p\sigma(3)$; hence, it is not identified here. The v = 1, 2, and 3 levels appear to have high (> 50%) UV quantum yields. For the v = 3 and 4 levels, direct assignment of quantum efficiencies is difficult because of spectral overlap. The $B'^2\Delta(4)$ level appears to fluoresce with about a 25% quantum efficiency. The v = 5 level overlaps the $4s\sigma(2)$ band, and the assignment of the fluorescence quantum yield is inconclusive.

Below 1520 Å, there is a precipitous drop in emission intensity from all states, as shown in Figure 4. The $B'^2\Delta(6)$ level is known to be highly perturbed by the $3d\delta(2)$ level; in fact, the former is "missing" in absorption (Dressler and Miescher 1965, Jungen 1966). Weak fluorescence at 1520 Å may be due to the strongly absorbing $K^2\Pi(4p)$ v = 1 Rydberg band, but we suspect that the emission originates from the $^2\Delta$ state. The $B'^2\Delta$ v = 7, 8, and 9 levels fluoresce only a small amount in the UV. They may predissociate, although earlier emission studies (Jungen and Miescher 1965, Jungen 1966) show strong B' → X emission up to v = 10. The fate of the molecules excited to the

$B'^2\Delta$ v = 7, 8, and 9 is puzzling. Visible emission has been observed from the $B'^2\Delta$ state to the $B^2\Pi$ state (Baer and Miescher 1953, Huber 1964) and to the $3p\pi$ state (visible to ir) (Ackermann 1971). The visible emission cross section measured in this study is not high enough to account for the decreased fluorescence cross section in the UV. The lower fluorescence cross section may be caused by predissociation.

The $F^2\Delta(d\delta)$ Rydberg state also fluoresces in the UV. From earlier studies, the v = 0, 1, 2, and 3 bands are found to emit upon discharge excitation. The $3d\delta(0)$ band overlaps the $3p\sigma(4)$ band so a definitive quantum yield assignment is not possible. At v = 1, the $3d\delta$ band is overlapped and perturbed by the $B^2\Delta(4)$ band, and again a quantum yield cannot be assigned. The $3d\delta(2)$ band is intense in absorption, but has only about a 2% UV quantum yield. At v = 3, the $3d\delta$ band still fluoresces, but at less than 0.5%. The $F^2\Delta \rightarrow C^2\Pi$ transition is known to occur in the ir, but its radiative rate is not likely to account for all the "missing" emission.

The $N^2\Delta(4d\delta)$ and $U^2\Delta(5d\delta)$ Rydberg states absorb farthest into the UV for the $^2\Delta$ states studied here. $N^2\Delta \rightarrow X^2\Pi$ emission has been observed from discharge excitation (Jungen, 1966), and we see weak UV emission at 1430 Å that may be attributed to the $4d\delta(1)$ band. Coincident in energy with the $5d\delta(0)$ band, we also observe somewhat stronger emission. No $U^2\Delta \rightarrow X^2\Pi$ emission spectra have been reported, but the general nature of the other $^2\Delta$ states implies that some fluorescence from the $5d\delta$ band is not unexpected.

At excitation wavelengths below 1410 Å, we observe no UV fluorescence. At these incident energies, NO is excited above its fourth dissociation limit (Gilmore 1965), and an ever-increasing fraction of states will predissociate. Figure 7 is a graphical representation of the approximate photo-

dissociation yield of NO in terms of its photoionization and fluorescence quantum yields. Between the first ionization limit of 1338 Å (9.266 eV) and 1520 Å, most of the molecules dissociate. At energies between 1520 Å and 1908 Å, the dissociation yield depends on the excited state symmetry. Watanabe et al (1967) measure a high photoionization yield at wavelengths shorter than 1338 Å, and there again the NO dissociation yield is low. Other absorption states that do not appear to fluoresce include the $B^2\Pi$ valence state, the $S^2\Sigma^+(5s\sigma)$ Rydberg state, and the $G^2\Sigma^-$ valence state.

5. CONCLUSION

The absorption cross sections measured here verify those of Watanabe et al (1967) below 1350 Å. At longer wavelengths, we have measured average absorption cross sections that can be related to the true cross section per rotational line.

UV fluorescence cross sections have been measured relative to our absorption cross sections and are subject to the same absolute magnitude adjustments from which the quantum yield for total UV fluorescence has been determined. Our fluorescence excitation spectra are consistent with previous fluorescence measurements and discharge studies. The decrease in emission intensity for some vibrational progressions may be attributed to predissociation, and in the case of the $B'^2\Delta$ state, this predissociation has been previously unrecognized. The UV quantum yields determined in this work are a quantitative indicator of the extent of predissociation in the complex manifold of NO electronic states and may prove helpful for further understanding the spectroscopy of NO as well as its aeronomic and interstellar photochemistry.

ACKNOWLEDGMENTS

The authors are grateful to the staff of the Synchrotron Radiation Center (SRC) of the University of Wisconsin, in particular, E. M. Rowe and R. Otte. We thank Dr. C. G. Olson for the use of the MacPherson monochromator. We also thank Dr. T. G. Slanger, Dr. D. L. Huestis and Dr. J. R. Peterson for helpful discussions, and Dr. F. Lahmani for communication of results prior to publication. J. A. Guest thanks Prof. R. N. Zare for financial support under NSF Grant PHY79-08694. The PDP 11/40 computer used to analyze the data was purchased under NSF Grant No. PYU76-14436. The SRC is supported by the National Science Foundation under Grant DMR-77-21888.

This work was supported by the National Aeronautics and Space Administration/Astrophysics Division under Contract NASW-3270.

TABLE 1. The Integrated Absorption Coefficients, Ko, for the Various NO Absorption Bands

Transition	Band	Ko(Bethke, 1959)	Ko (This Work)
		cm^{-2} atm^{-1}	cm^{-2} atm^{-1}
$B^2\Pi - X^2\Pi$	$\beta(12,0)$	54.9 (3)[a]	63 (3)[a]
$A^2\Sigma^+ - X^2\Pi$	$\gamma(3,0)$	8.57 (3)	9.7 (3)
$C^2\Pi - X^2\Pi$	$\delta(0,0)$ $+\beta(7,0)$	59.2 (3)	93 (3)
	$\delta(1,0)$ $+\beta(10,0)$	137.0 (3)	170 (3)
	$\delta(2,0)$	65.2 (3)	120 (3)
$D^2\Sigma^+ - X^2\Pi$	$\varepsilon(0,0)$ $+\gamma(4,0) + \beta(8,0)$	60.4 (3)	63 (3)
	$\varepsilon(1,0)$ $+\gamma(5,0)$	109. (3)	130 (3)
	$\varepsilon(2,0)$ $+\gamma(6,0) + \beta(13,0)$	78.9 (3)	86 (3)

[a](3) means 10^3

REFERENCES

Ackermann F 1971 Can. J. Phys. 49 76-89

Asscher M and Haas Y 1978 Chem. Phys, Lett. 59 231-6

Baer P and Miescher E 1953 Helv. Phys. Acta 26 91-110

Benoist D'Azy O Lopez-Delgado R and Tramer A 1975 Chem. Phys 9 327-38

Bethke G W 1959 J. Chem. Phys. 31 662-8

Brzozowski J Erman P and Lyyra M 1976 Physica Scripta 14 290-7

Callear A B and Pilling M J 1970 Trans. Faraday Soc. 66 1618-34; ibid 1886-906

Cieslik S and Nicolet M 1973 Planet. Space Sci. 21 925-38

Dressler K and Miescher E 1965 Astrophys. J. 141 1266-83

Engleman Jr R Rouse P E Peet H M and Baiamonte V D 1970 LASL Report LA-4364

Farmer A J D Fabian W Lewis B R Lokan K H and Haddad G N 1968 J. Quant Spectrosc. Radiat. Transfer 8 1739-46

Farmer A J D Hasson V and Nicholls R W 1972 J. Quant. Spectrosc. Radiat. Transfer 12 627-33; ibid 635-8

Frederick J E and Hudson R D 1979 Atmo. Sci. 36 737-45

Gilmore F R 1965 J. Quant. Spectrosc. Radiat. Transfer 5 369-90

Huber M 1964 Helv. Phys. Acta 37 329-47

Jungen C 1966 Can. J. Phys. 44 3197-216

Jungen C and Miescher E 1965 Astrophys. J. 142 1660-1

Lagerqvist A and Miescher E 1966 Can. J. Phys. 44 1525-39

Lahmani F Lardeux C and Solgadi D 1981 to be published

Lee L C 1980 J. Chem. Phys. 72 4334-40

Lee L C and Guest J A 1981 to be published

Liszt H S and Turner B E 1978 Astrophys. J. 224 L73-6

Loftus A and Miescher E 1964 Can. J. Phys. 42 848-59

Marmo F F 1953 J. Opt. Soc. Am. 43 1186-90

Miescher E 1966 J. Mol. Spec. **20** 130-140

Miescher E 1971 Can. J. Phys. **49** 2350-65

Miescher E and Alberti F 1976 J. Chem. Phys. Ref. Data **5** 309-17

Miescher E and Huber K P 1976 Int. Rev. Sci. (Ser. 2) Spectroscopy Ramsay D A, Ed **3** 37-73

Nicholls R W 1964 J. Res. NBS A **68A** 535-40

Ng C Y Mahan B H and Lee Y T 1976 J. Chem. Phys. **65** 1956-61

Slanger T G 1980 private communication

Spindler Jr R J Isaacson L and Wentink Jr T 1970 J. Quant. Spectrosc. Radiat. Transfer **10** 621-8

Tanaka Y 1953 J. Chem. Phys. **21** 788-93

Watanabe K Matsunaga F M and Sakai H 1967 Appl. Opt. **6** 391-6

Young R A Black G and Slanger T G 1968 J. Chem. Phys. **48** 2067-70

FIGURE CAPTIONS

Fig. 1 Attenuation of photon fluxes at wavelengths 1406, 1499, 1605, 1731, and 1829 Å by NO of pressure up to 40 mtorr. I_o and I are the incident and attenuated light intensities, respectively.

Fig. 2 The photon flux for the synchrotron radiation in the 1050-2100 Å region that enters the gas cell. The efficiency for the solar blind photomultiplier in the 1130-3500 Å region is also shown.

Fig. 3 Photoabsorption cross section of NO in the 1060-1350 Å region. The wavelength positions of various states given by Miescher (1966), Miescher and Alberti (1976), Miescher and Huber (1976), and Ng *et al.* (1976) are indicated.

Fig. 4 Photoabsorption and fluorescence cross sections of NO in the 1350-1510 Å region. The wavelength positions of various states given by Dressler and Miescher (1965), Jungen (1966), Lagerquist and Miescher (1966), Lofthus and Miescher (1964), Miescher (1966), Miescher and Alberti (1976), and Miescher and Huber (1976) are indicated.

Fig. 5 Photoabsorption and fluorescence cross sections of NO in the 1510-1720 Å region. The wavelength positions of various states given by Dressler and Miescher (1965), Jungen (1966), Lagerquist and Miescher (1966), Miescher (1971), and Miescher and Huber (1976) are indicated.

Fig. 6 Photoabsorption and fluorescence cross sections of NO in the 1720-1970 Å region. The wavelength positions of various states given by Miescher and Huber (1976) and Tanaka (1953) are indicated.

Fig. 7 The fluorescence, photoionization, and photodissociation yields for the excitation photon wavelengths in the 1000-2000 Å region. The photoionization yields were given by Watanabe et al. (1967). The photodissociation yield is determined by the difference of unity and the fluorescence or photoionization yield.

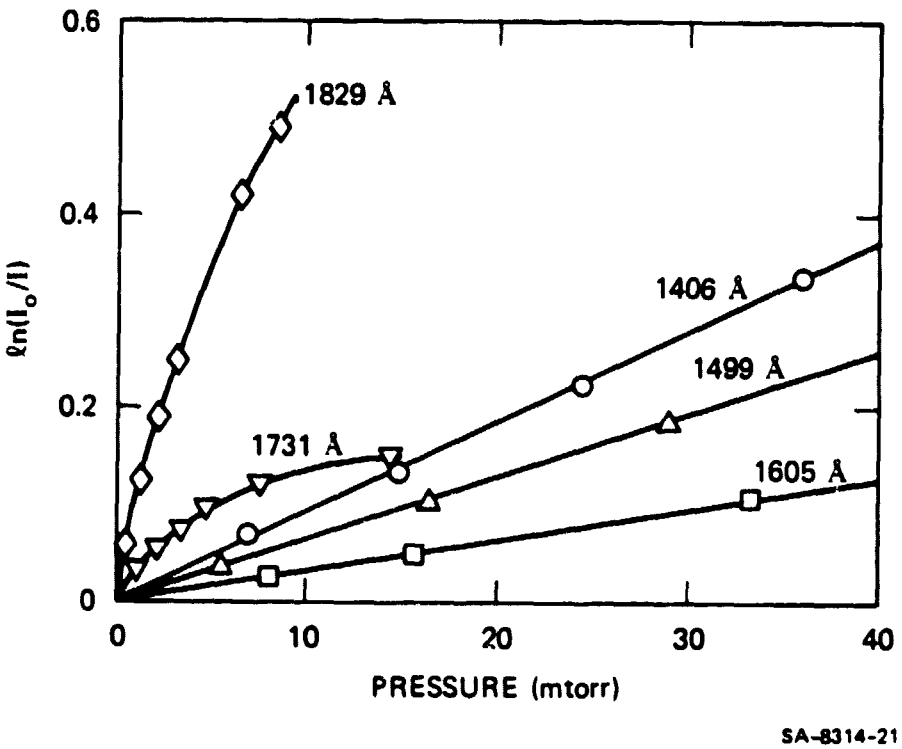
0.6
0.4
0.2
0
0
10
20
30
40
ℓn(I$_o$/I)
PRESSURE (mtorr)
1829 Å
1406 Å
1499 Å
1731 Å
1605 Å
SA-8314-21

Figure 1

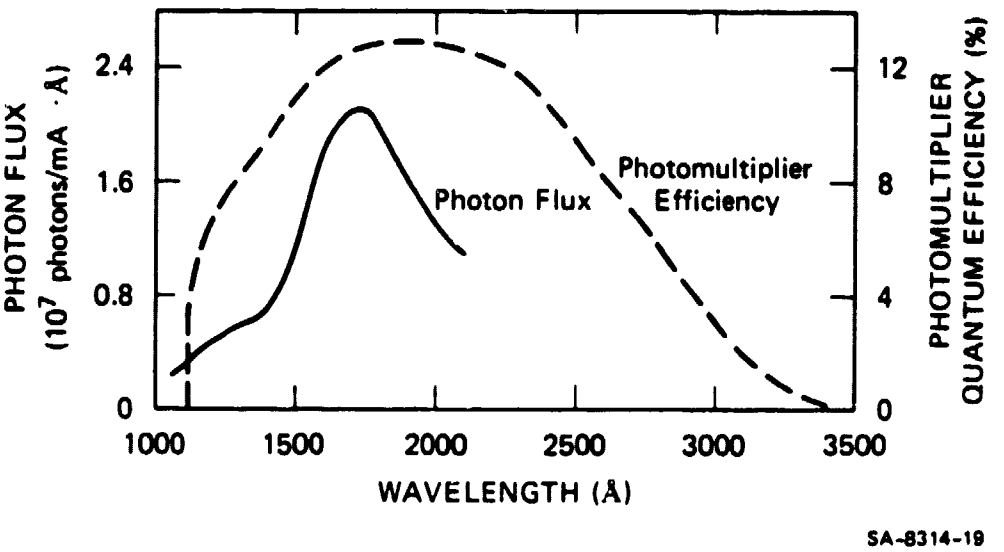
PHOTON FLUX
(10^7 photons/mA · Å)
2.4
1.6
0.8
0
PHOTOMULTIPLIER
QUANTUM EFFICIENCY (%)
12
8
4
0
Photon Flux
Photomultiplier
Efficiency
1000
1500
2000
2500
3000
3500
WAVELENGTH (Å)
SA-8314-19

Figure 2

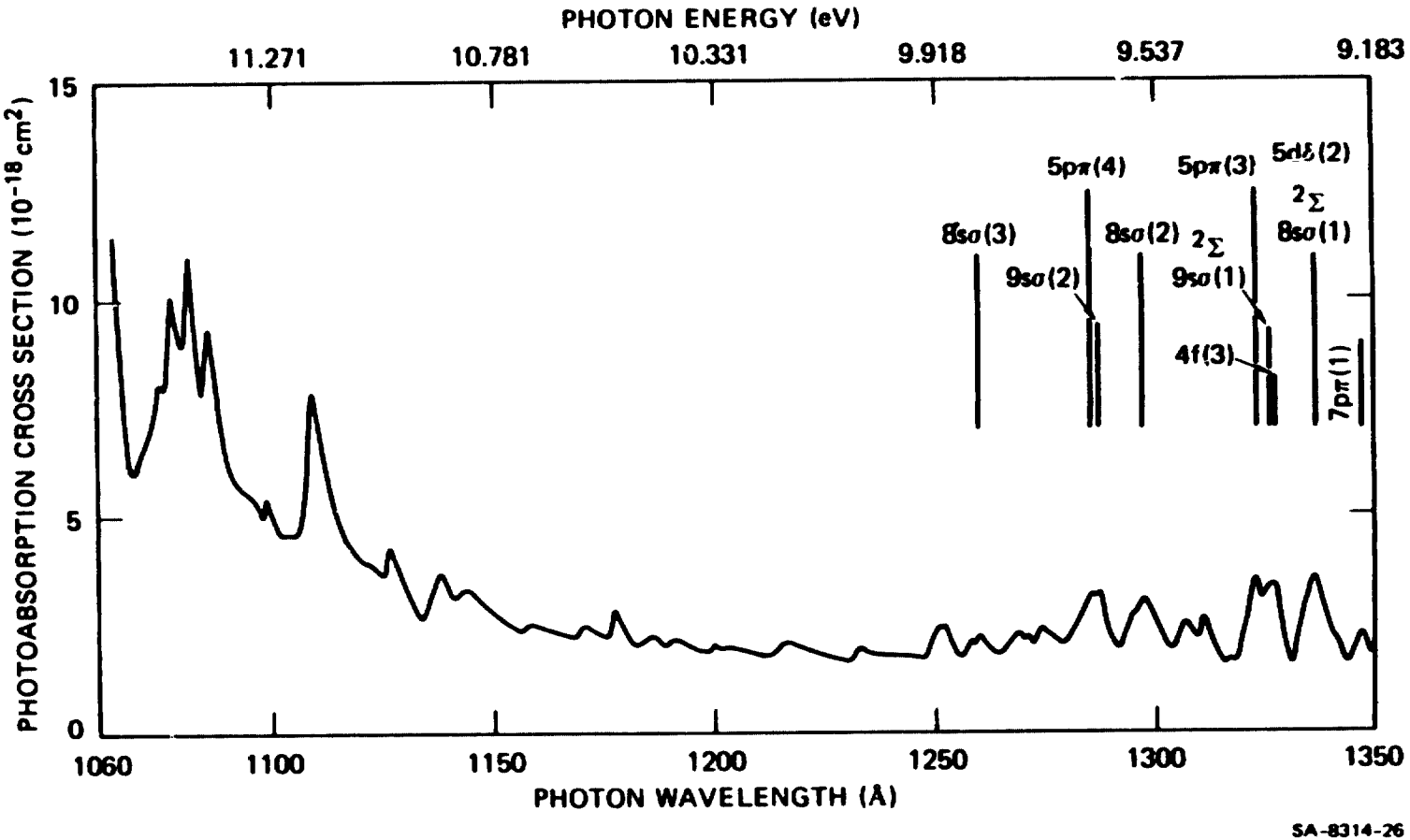
PHOTON ENERGY (eV)
11.271
10.781
10.331
9.918
9.537
9.183
PHOTOABSORPTION CROSS SECTION (10^{-18} cm^2)
15
10
5
0
1060
1100
1150
1200
1250
1300
1350
PHOTON WAVELENGTH (Å)
8sσ(3)
9sσ(2)
5pπ(4)
8sσ(2)
$^2\Sigma$
9sσ(1)
5pπ(3)
4f(3)
5dδ(2)
$^2\Sigma$
8sσ(1)
7pπ(1)
SA-8314-26

Figure 3

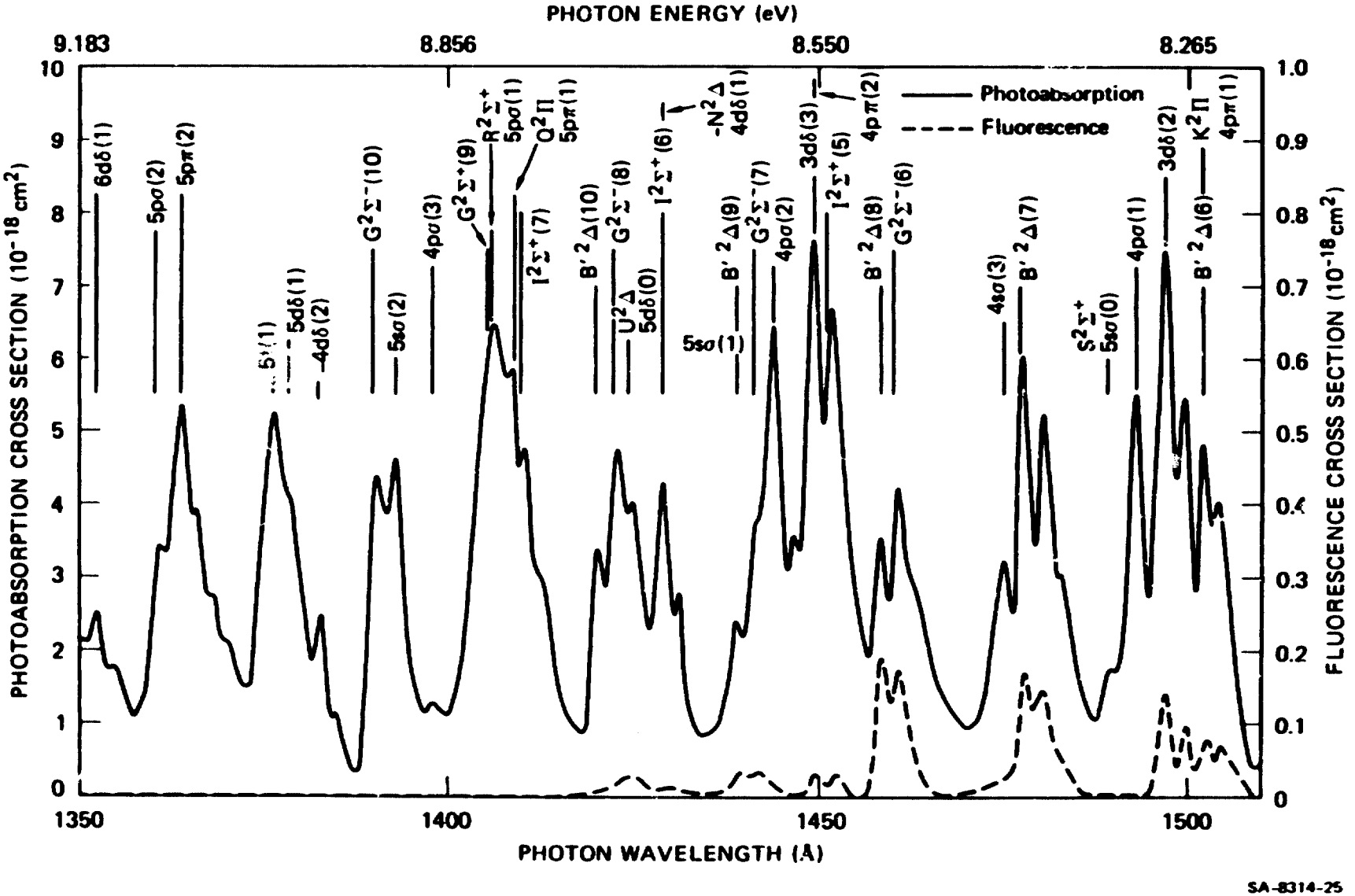
PHOTON ENERGY (eV)
9.183
8.856
8.550
8.265
PHOTOABSORPTION CROSS SECTION (10^{-18} cm^2)
FLUORESCENCE CROSS SECTION (10^{-18} cm^2)
Photoabsorption
Fluorescence
PHOTON WAVELENGTH (Å)
1350
1400
1450
1500
6dδ(1)
5pσ(2)
5pπ(2)
5dδ(1)
4dδ(2)
G$^2\Sigma^-$(10)
5sσ(2)
4pσ(3)
G$^2\Sigma^+$(9)
R$^2\Sigma^+$
5pσ(1)
Q$^2\Pi$
5pπ(1)
I$^2\Sigma^+$(7)
B′ $^2\Delta$(10)
U$^2\Delta$
G$^2\Sigma^-$(8)
5dδ(0)
I$^2\Sigma^+$(6)
-N$^2\Delta$
4dδ(1)
5sσ(1)
B′ $^2\Delta$(9)
G$^2\Sigma^-$(7)
4pσ(2)
3dδ(3)
I$^2\Sigma^+$(5)
4pπ(2)
B′ $^2\Delta$(8)
G$^2\Sigma^-$(6)
4sσ(3)
B′ $^2\Delta$(7)
S$^2\Sigma^+$
5sσ(0)
4pσ(1)
3dδ(2)
B′ $^2\Delta$(6)
K$^2\Pi$
4pπ(1)
SA-8314-25

Figure 4

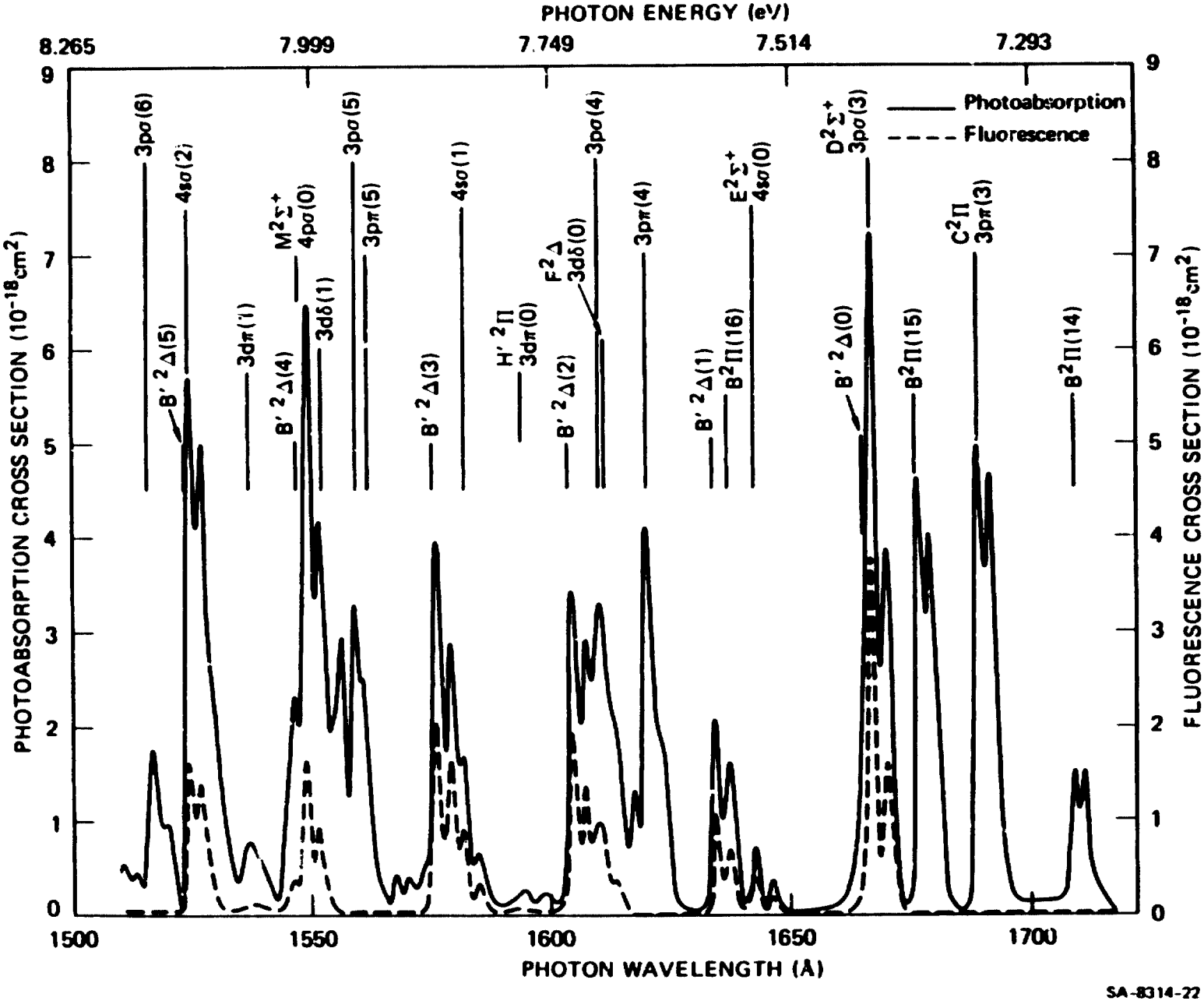
PHOTON ENERGY (eV)
8.265
7.999
7.749
7.514
7.293
Photoabsorption
Fluorescence
PHOTOABSORPTION CROSS SECTION (10^{-18}cm^2)
FLUORESCENCE CROSS SECTION (10^{-18}cm^2)
PHOTON WAVELENGTH (Å)
1500
1550
1600
1650
1700
3pσ(6)
B′ $^2\Delta$(5)
4sσ(2)
3dπ(1)
B′ $^2\Delta$(4)
M$^2\Sigma^+$ 4pσ(0)
3dδ(1)
3pσ(5)
3pπ(5)
B′ $^2\Delta$(3)
4sσ(1)
H′ $^2\Pi$ 3dπ(0)
B′ $^2\Delta$(2)
F$^2\Delta$ 3dδ(0)
3pσ(4)
3pπ(4)
B′ $^2\Delta$(1)
B$^2\Pi$(16)
E$^2\Sigma^+$ 4sσ(0)
D$^2\Sigma^+$ 3pσ(3)
B′ $^2\Delta$(0)
B$^2\Pi$(15)
C$^2\Pi$ 3pπ(3)
B$^2\Pi$(14)
SA-8314-22

Figure 5

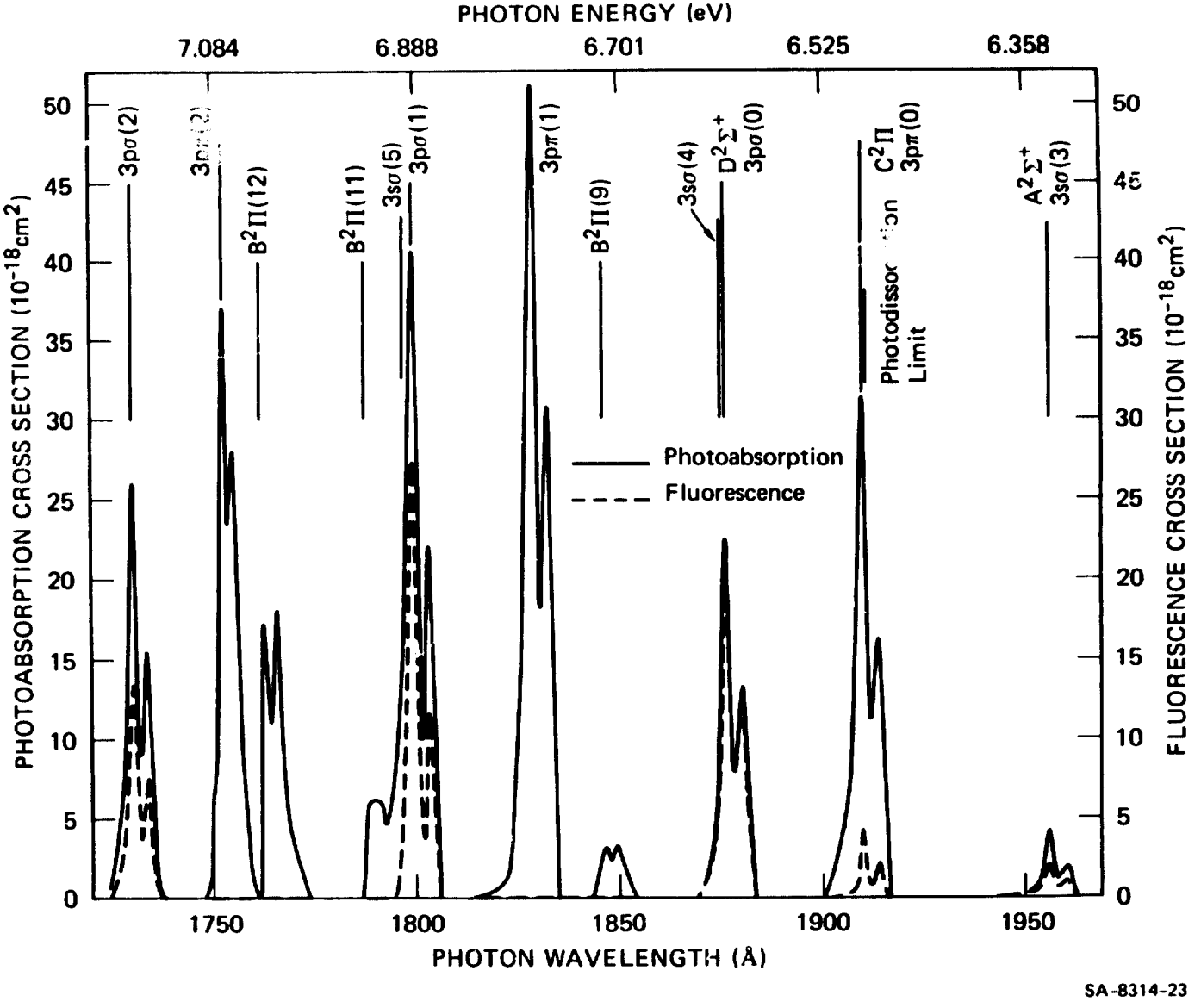
PHOTON ENERGY (eV)
7.084
6.888
6.701
6.525
6.358
PHOTOABSORPTION CROSS SECTION (10^{-18}cm^2)
FLUORESCENCE CROSS SECTION (10^{-18}cm^2)
0
5
10
15
20
25
30
35
40
45
50
1750
1800
1850
1900
1950
PHOTON WAVELENGTH (Å)
3pσ(2)
3pπ(2)
B^{2}Π(12)
B^{2}Π(11)
3sσ(5)
3pσ(1)
3pπ(1)
B^{2}Π(9)
3sσ(4)
D^{2}Σ$^+$
3pσ(0)
C^{2}Π
3pπ(0)
Photodissociation
Limit
A^{2}Σ$^+$
3sσ(3)
Photoabsorption
Fluorescence
SA-8314-23

Figure 6

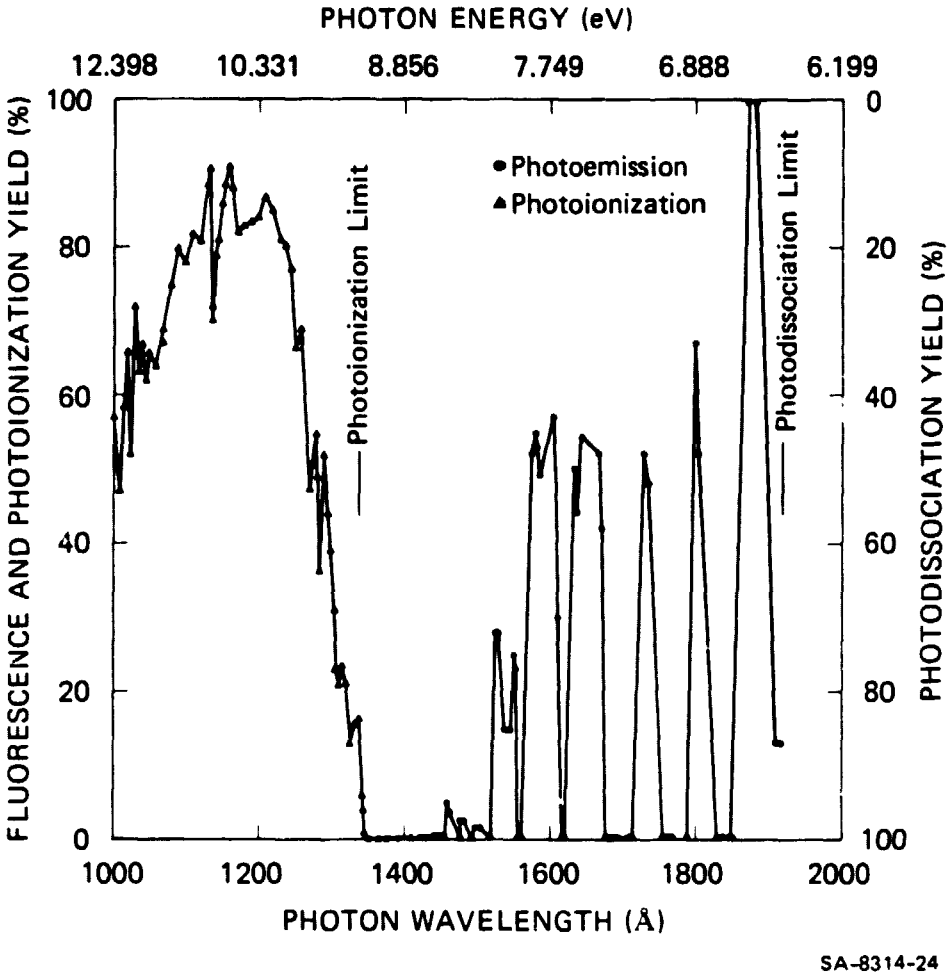
PHOTON ENERGY (eV)
12.398
10.331
8.856
7.749
6.888
6.199
FLUORESCENCE AND PHOTOIONIZATION YIELD (%)
PHOTODISSOCIATION YIELD (%)
100
80
60
40
20
0
0
20
40
60
80
100
Photoionization Limit
Photodissociation Limit
Photoemission
Photoionization
1000
1200
1400
1600
1800
2000
PHOTON WAVELENGTH (Å)
SA-8314-24

Figure 7